Semenogelin-1 Inhibition of Mouse Sperm Hyperactivation Reveals Two Functional Domains Modulating CatSper Channel

Noemia A. P. Mariani[1], Natália C. M. Santos[1], Juliana J. Andrade[1], Alexandre D. Andrade[1], Beatriz Rezende[1], Tomás J. Steeman[2], Analia G. Novero[2], José C. de Lima-Junior[3], Giulia Calderaro[1], Ana Clara F. Themer[1], Hélio Kushima[1], Mariano G. Buffone[5], Darío Krapf[2], Polina V. Lishko[3,4], Erick J. R. Silva[1]*.

[1]Department of Biophysics and Pharmacology, Biosciences Institute of Botucatu, São Paulo State University, Botucatu, SP, Brazil; [2]Institute of Molecular and Cellular Biology of Rosario, Rosario, SF, Argentina; [3]Department of Cell Biology and Physiology, Washington University in St. Louis, School of Medicine, St. Louis, MO, United States; [4]Center for the Investigation of Membrane Excitability Diseases (CIMED), WashU Medicine, St. Louis, MO, United States; [5]Institute of Biology and Experimental Medicine, Buenos Aires, BA, Argentina.

* To whom correspondence should be addressed: E-mail: ejr.silva@unesp.br; Phone: +55 14 3880-0223.

Running title: SEMG1 inhibition of sperm hyperactivation.

Keywords: Sperm motility, Epididymal protease inhibitor, EPPIN, Spermatozoon, Ion Channels, Seminal Plasma, Semenogelins.

Abstract

Seminal plasma proteins are essential for preserving sperm survival and functional integrity after ejaculation. Semenogelin-1 (SEMG1) is the predominant seminal plasma protein and the major structural component of the semen coagulum and copulatory plug in humans and rodents, respectively. On the sperm surface, SEMG1 binds to EPPIN (epididymal protease inhibitor), transiently suppressing the acquisition of sperm motility after ejaculation and preventing sperm hyperactivation. However, the molecular mechanisms by which SEMG1 inhibits sperm hyperactivation remain unclear. We hypothesize that SEMG1 exerts its effects through inhibition of CatSper, a sperm-specific calcium channel crucial for hyperactivation. Supporting this, we observed that recombinant mouse SEMG1 (mSEMG1) inhibited both progressive motility and hyperactivation in a concentration-dependent manner. Notably, the latter was not recovered with NH_4Cl-induced alkalinization, suggesting that the effects of mSEMG1 are downstream of capacitation-associated intracellular alkalinization. Electrophysiological recordings revealed that mSEMG1 impaired CatSper currents at physiologically relevant concentrations. Recombinant mSEMG1 truncations mSEMG1$^{Q32\text{-}V118}$ and mSEMG1$^{R98\text{-}G375}$, but not mSEMG1$^{Y221\text{-}G375}$, independently inhibited sperm hyperactivation and CatSper currents similar to full-length mSEMG1. However, only mSEMG1$^{R98\text{-}G375}$ displayed similar EPPIN-binding capacity comparable to full-length mSEMG1, whereas mSEMG1$^{Q32\text{-}V118}$ and mSEMG1$^{Y221\text{-}G375}$ showed only minor binding. Our findings reveal that two distinct functional domains of mouse SEMG1, spanning the Q32-V118 and R98-S220regions, inhibit sperm hyperactivation by targeting the CatSper channel, both independently and dependent on EPPIN binding. These functional domains represent promising prototypes for the design of spermiostatic molecules, offering additional avenues for non-hormonal male contraception.

Introduction

To successfully fertilize the egg, spermatozoa must undergo their final maturation within the female reproductive tract, in a process named capacitation (1–3). Sperm capacitation entails a complex cascade of molecular events, including cholesterol efflux from the plasma membrane, tyrosine phosphorylation of sperm proteins, an increase in intracellular pH (pH_i), a rise in intracellular Ca^{2+} concentrations ($[Ca^{2+}]_i$), and membrane hyperpolarization. Sperm capacitation allows spermatozoa to undergo acrosome exocytosis upon stimulation and to transition from progressive motility to a whip-like flagellar motion known as hyperactivation (1, 4–8).

Among the molecular pathways involved in sperm hyperactivation, the rise in intracellular Ca^{2+} levels is critical (9). Even though multiple mechanisms promote Ca^{2+} influx in spermatozoa, the activation of the voltage-dependent and alkalinization-activated Ca^{2+} channel CatSper is considered the most relevant (10). The CatSper channel consists of a complex of at least fourteen proteins: four pore-forming subunits (CatSper1–4) and 10 accessory subunits (CatSper β, γ, δ, ε, ζ τ, η, θ, EFCAB9, and transporter SLCO6C1) (10–12). This large multiprotein complex, known as CatSpermasome, is arranged as four longitudinal lines spanning the entire length of the sperm principal piece (4, 12–14), facilitating structural and functional coupling between CatSper complexes and triggering powerful Ca^{2+} waves along the sperm flagellum (14). Notably, CatSper deficiency in men and rodents leads to infertility due to a failure of sperm hyperactivation, while no other phenotypical abnormalities are observed (4, 10, 15–18).

While sperm hyperactivation is crucial for fertilization, it must remain tightly regulated until spermatozoa reach the oviduct (19). In this context, seminal plasma components play critical roles in modulating sperm hyperactivation and other capacitation-associated events (20). Semenogelin-1 (SEMG1), the predominant protein in seminal plasma, is secreted by the seminal vesicles and incorporated onto the sperm surface during ejaculation through its interaction with EPPIN in both humans and rodents (21–24). SEMG1 binds to freshly ejaculated spermatozoa, acting as a decapacitation factor and blocking sperm motility, hyperactivation, and acrosome exocytosis (25–31). In humans, this inhibitory effect is maintained until the serine protease prostate-specific antigen (PSA) cleaves SEMG1, resulting in semen liquefaction and activation of sperm motility (32). Furthermore, SEMG1 promotes sperm survival in the uterus, as evidenced by the low viability of spermatozoa from *Semg1*$^{-/-}$ mice collected from the female reproductive tract during natural mating, causing a severe subfertility phenotype (33). Together, these findings indicate that SEMG1 has a dual role of protecting and modulating sperm function and metabolism during their journey through the female reproductive tract. However, the precise molecular mechanisms underlying SEMG1's roles and the contribution of EPPIN binding to these effects remain poorly understood.

Initial studies have shown inhibitory effects of SEMG1 on sperm pH_i and $[Ca^{2+}]_i$ (34). Building upon these findings, we hypothesize that SEMG1 inhibits CatSper activity, thereby affecting Ca^{2+} homeostasis and downstream pathways required for sperm hyperactivation. To test this hypothesis, we investigated the effects of mouse SEMG1 (mSEMG1) on sperm motility,

hyperactivation, and CatSper activity. We further characterized the functional domains of SEMG1 and the relevance of EPPIN binding in mediating its effects. Our results revealed that mSEMG1 inhibits hyperactivation by modulating CatSper currents, an effect mediated by two independent domains within the Q32-V118 and R98-S220 sequences. Notably, only the R98-S220 sequence bound EPPIN, indicating that SEMG1 controls sperm hyperactivation by multiple mechanisms, both dependent and independent of EPPIN binding. Our results highlight the essential role of SEMG1 in preventing premature sperm hyperactivation and offer promising avenues for exploring its functional domains as prototypes for the rational design of ligands with male contraceptive applications targeting spermatozoa.

Results

Mouse SEMG1 inhibits sperm progressive and hyperactivated motilities

The sperm motility pattern changes from progressive to hyperactivated upon capacitation (35, 36). Previous studies have shown that both human and mouse SEMG1 can regulate sperm function, including motility (25, 28, 37). To gain insights into the effects of SEMG1 on sperm swimming behavior, we incubated murine spermatozoa isolated from the cauda epididymidis in capacitating medium, in either the absence (control) or in the presence of increasing concentrations of full-length recombinant mouse SEMG1 (mSEMG1; Q32-G375). mSEMG1 reduced sperm motility only at 25 µM (~25% inhibition) after 20 min ($p=0.0005$) and 120 min ($p=0.011$) of incubation compared to the control (Fig. 1A, Fig. S1, Video S1). Concurrently, mSEMG1 increased the percentage of slow-moving spermatozoa at 10 µM ($p=0.026$) and 25 µM ($p=0.001$) after 20 min of incubation compared to the control (Fig. 1B, Fig. S1). mSEMG1 did not affect sperm viability at the concentrations tested, confirming that its effects on sperm motility were not associated with sperm death (Fig. 1C).

mSEMG1 displayed a more potent effect on hyperactivated motility by inhibiting it in a concentration-dependent manner with an IC_{50} of 5.2 µM (95% confidence interval; CI 1.3–21.2 µM). The maximum inhibition of ~90% was reached at 25 µM ($p = 0.0003$) after 120 min, compared to the control (Fig. 2A, B). Consistently, 25 µM mSEMG1 decreased curvilinear velocity (VCL, $p = 0.006$) and amplitude of lateral head displacement (ALH, $p = 0.005$), kinematic parameters associated with vigorous sperm movements (38) (Fig. 2C). Notably, mSEMG1 effects on hyperactivation were not rescued by intracellular alkalization induced by NH_4Cl (Fig. 2D), a condition that enhance sperm hyperactivation via alkalinization evoked activation of CatSper (39, 40) (Fig. 2D). Similarly, mSEMG1 inhibited progressive motility (IC_{50} 10.1 µM, 95% CI 2.6–38.5 µM), and decreased both average path velocity (VAP) and straight-line velocity (VSL), kinematic parameters associated with sperm progressiveness (Fig. S2). Altogether, these results indicate that mSEMG1 inhibits mouse sperm progressive motility and hyperactivation by modulating signaling pathways downstream of intracellular alkalinization.

Mouse SEMG1 is a CatSper channel inhibitor

Activation of CatSper channel leads to a rise in intracellular Ca^{2+} concentration, which is essential for the development of hyperactivated motility in both murine and human spermatozoa (16, 41, 42). Thus, we decided to explore whether mSEMG1 inhibits hyperactivation by affecting the CatSper channel. To do so, we conducted whole-cell patch clamp experiments using non-capacitated murine spermatozoa to record CatSper currents ($I_{CatSper}$) in the absence or presence of mSEMG1.

$I_{CatSper}$ were elicited by voltage ramps from -80 to +80 mV from a holding potential of 0 mV (Fig. 3A). Under these conditions, no CatSper current was detected in a high-saline (HS) extracellular bath solution containing Ca^{2+} and Mg^{2+} (Table S1), which represents the baseline recording (Fig. 3B). The remaining current under this condition was attributed to a leak current and was negligible. Upon perfusion with divalent-free Cs^{+}-based (DVF) bath solution (Table S2), the characteristic monovalent CatSper current was recorded, as previously described (43, 44) (Fig. 3B) . Following the DVF perfusion, sperm cells were exposed to 5 µM mSEMG1, which suppressed both inward and outward CatSper currents (Fig. 3B, C). After subtracting the leak currents, the averaged (± standard error of the mean) control inward $I_{CatSper}$ in DVF at -80 mV was 218.4 ± 31.7 pA (Fig. 3B). Under the same conditions, exposure to 5 µM mSEMG1 inhibited the inward $I_{CatSper}$ to 150.8 ± 23.4 pA (~31% suppression; $p = 0.019$) (Fig. 3B). No currents were detected when spermatozoa from *CatSper1*$^{-/-}$ mice were tested either in the absence or presence of mSEMG1 (Fig. 3B, insert). Notably, mSEMG1 inhibition was reversible as CatSper conductance recovered upon continuous washing in DVF (177.0 ± 17.2 pA; $p = 0.378$) (Fig. 3B).

In addition to intracellular alkalization, CatSper is sensitive to membrane voltage (4, 39). During capacitation, the sperm plasma membrane undergoes hyperpolarization via the sperm-specific and pH-sensitive K^{+} channel Slo3, which in turn is activated by alkaline intracellular pH (45). Therefore, we tested the effect of reduced $I_{CatSper}$ caused by mSEMG1 on membrane potential (Em) during sperm capacitation. As expected, capacitated spermatozoa displayed a more negative membrane potential in comparison to non-capacitated spermatozoa (Fig. 3D, Fig. S3). Capacitation-induced membrane hyperpolarization was not affected in the presence of 10 µM mSEMG1 (Fig. 3D, Fig. S3). These results indicate that mSEMG1 inhibits CatSper activity at low micromolar concentrations similar to those required to inhibit sperm hyperactivation, without affecting the Em. In the normal physiological scenario, mouse SEMG1 is present in the seminal plasma at higher concentrations (≥ 25 µM) than its IC_{50} for inhibiting hyperactivation in our experimental conditions (26). Thus, SEMG1 is likely able to prevent premature hyperactivation by blocking CatSper in murine spermatozoa, either through mechanisms independent of intracellular alkalinization or Em, or by directly binding to the channel.

Mouse SEMG1 Q32-V118 and R98-S220 sequences independently contribute to the inhibition of sperm hyperactivation and CatSper currents

Despite the low conservation in their primary sequences, both human and mouse SEMG1 exhibit a single cysteine residue (C239 in human SEMG1 and C97 in mouse SEMG1), as well as internal repetitive amino acid sequences (46). Downstream of the cysteine residue, mouse SEMG1 contains two 31-amino acid repeats (K119-S149 and K177-S207) and multiple short repeats of two (KS), three (GGS), or six-eight (QVKSSVSQ or QVKSSGSQ) amino acid residues that become less frequent toward its C-terminal region (Fig. 4A). Previous studies demonstrated that sequences within human SEMG1 that are part of long repeats and flank the cysteine residue are essential for its interaction with spermatozoa, EPPIN binding, and modulation of sperm motility (25, 37). Based on these observations, we obtained three truncated mSEMG1 constructs (i) mSEMG1$^{Q32\text{-}V118}$, which contains its unique cysteine residue, (ii) mSEMG1$^{R98\text{-}G375}$, which lacks the cysteine residue but includes the two long repeats, and (iii) mSEMG1$^{Y221\text{-}G375}$, which lacks both the cysteine residue and the long repeats (Fig. 4A), allowing us to evaluate the relevance of these sequences to the inhibition of sperm hyperactivation.

We observed that neither of the truncated mSEMG1 constructs affected sperm motility in a significant manner (Fig. 4B). Nevertheless, mSEMG1$^{Q32\text{-}V118}$ and mSEMG1$^{R98\text{-}G375}$, but not mSEMG1$^{Y221\text{-}G375}$, inhibited hyperactivated motility compared to the control ($p = 0.004$ and 0.028, respectively) to a similar extent as the full-length mSEMG1 (Fig. 4B and C, Fig. S4, Video S2). mSEMG1$^{Q32\text{-}V118}$ also reduced the associated kinematic parameter VCL ($p = 0.029$), and a similar trend was observed for mSEMG1$^{R98\text{-}G375}$ ($p = 0.084$) (Fig. 4C). Consistent with these findings, both mSEMG1$^{Q32\text{-}V118}$ and mSEMG1$^{R98\text{-}G375}$ suppressed inward and outward $I_{CatSper}$ (Fig. 5A and B, Fig. S5). mSEMG1$^{Y221\text{-}G375}$ also inhibited CatSper, albeit to a lesser extent than the rest of the truncated constructs (Fig. 5A-C, Fig. S5). At 5 µM concentration, mSEMG1$^{Q32\text{-}V118}$, mSEMG1$^{R98\text{-}G375}$, and mSEMG1$^{Y221\text{-}G375}$ suppressed the inward $I_{CatSper}$ at -80 mV to values equivalent to ~56%, ~66%, and ~77% of those observed with their respective controls, corresponding to mean differences of of 93.6 ($p = 0.007$), 108.6 ($p < 0.0001$), and 55.9 pA ($p = 0.011$), respectively (Fig. 5A-C, Fig. S5). These results indicate that sequences within the mSEMG1 Q32-V118 and R98-S220 regions, which encompass cysteine and the long repeats, contain domains sufficient to inhibit sperm hyperactivation through CatSper inhibition.

Mouse SEMG1 R98-G220 sequence contains the main EPPIN binding domain

Our previous study demonstrated the co-immunoprecipitation and co-localization of SEMG1 and EPPIN in mouse spermatozoa pre-incubated with seminal vesicle fluid, suggesting that EPPIN serves as a docking site for SEMG1 on the mouse sperm surface (21). Here, we confirmed the interaction between mouse EPPIN and SEMG1 using the AlphaScreen (Amplified Luminescent Proximity Homogeneous Assay Screen) assay (Fig. 6A), which has been previously employed to investigate the binding of human EPPIN and SEMG1 (22, 37). Using mSEMG1 and full-length

recombinant mouse EPPIN (mEPPIN; L24-T134), we observed a maximum interaction signal peaking at 2 hrs and remaining stable for at least 8 hrs (Fig. 6B). The interaction signals showed a concentration-dependent pattern when mSEMG1 and mEPPIN were titrated, with calculated EC_{50} (95% CI) of 23.6 nM (20.0–27.8 nM) and 1.0 nM (0.3–3.3 nM), respectively (Fig. 6C). Interestingly, when recombinant human SEMG1 (hSEMG1, G26-R281) replaced mSEMG1, we observed a concentration-dependent saturable binding curve, with a calculated EC_{50} of 8.3 nM (6.8–18.5 nM), confirming the conservation of the EPPIN binding sites in human and mouse SEMG1 sequences (Fig. S6).

To map the EPPIN binding site, we tested the mEPPIN binding capacity of our truncated mSEMG1 constructs. $mSEMG1^{R98\text{-}G375}$ showed a mEPPIN binding capacity similar to the full-length mSEMG1, both displaying a comparable specific signal (Fig. 6D). In contrast, we observed a reduction in the specific signal by ~80% ($p < 0.0001$) and ~69% ($p < 0.0001$) for $mSEMG1^{Q32\text{-}V118}$ and $mSEMG1^{Y221\text{-}G375}$ in comparison to full-length mSEMG1, respectively (Fig. 6D).

In addition, the removal of mouse EPPIN Kunitz domain in a C-terminal truncation lacking residues C69-T134 resulted in a reduction in the specific signal by ~75% ($p = 0.001$) compared to that detected with full-length EPPIN (Fig. 6E). Competition assays using anti-EPPIN antibodies Q20E and S21C, that recognized epitopes within EPPIN WFDC and Kunitz domains, respectively, reduced the specific signal of the binding of mEPPIN and mSEMG1 in a concentration-dependent manner with IC_{50} values of 3.0 nM (0.2–34.3 nM) and 95.6 nM (20.6–443.6 nM), respectively (Fig. S7). Altogether, these results demonstrate that the sequence R98-S220 of mSEMG1 contains the major mEPPIN binding domain and that both WFDC and Kunitz domains of mEPPIN are involved in mSEMG1 binding.

Discussion

During ejaculation, SEMG1 coats the sperm surface by interacting with EPPIN (21, 22, 37), thereby modulating sperm motility and preventing capacitation-associated events, such as hyperactivation and acrosome exocytosis (25, 26, 28, 34, 47). However, the underlying mechanisms governing the effects of SEMG1 on sperm function remain elusive. Here, we demonstrate that mSEMG1 inhibited sperm hyperactivation at concentrations at least 200-fold lower than those previously reported (28), highlighting SEMG1 as a potent, endogenous inhibitor of sperm hyperactivation. Moreover, we reveal that mouse SEMG1 contains two distinct functional domains – within the Q32-V118 and R98-S220 regions – which inhibit sperm hyperactivation at physiological concentrations by targeting CatSper. Since only the R98-S220 sequence is required for EPPIN binding, our data indicate that SEMG1 operates through both EPPIN-dependent and independent mechanisms to regulate sperm hyperactivation.

During capacitation, murine spermatozoa experience a pH_i shift from acidic to alkaline, primarily driven by Na^+/H^+ exchangers (NHEs) (48, 49). This event is crucial for the activation of sperm-specific ion channels, such as CatSper, which in turn leads to a rise in $[Ca^{2+}]_i$ (5, 10). Ca^{2+}

influx through CatSper plays a fundamental role in male reproduction, as the channel dysfunction leads to male infertility associated with hyperactivation failure in both humans and mice (50). While previous reports have demonstrated that the inhibition of sperm motility by SEMG1 was related to a decrease in $[Ca^{2+}]_i$ (34), the direct association of CatSper in this process has not been clarified. As shown herein, mSEMG1 exerts inhibitory effects on hyperactivation through inhibition of CatSper currents, thereby revealing a novel regulatory mechanism for CatSper activity promoted by a seminal plasma protein.

Given that intracellular alkalization is a well-established trigger for CatSper activation and sperm hyperactivation (39), we investigated whether pharmacologically induced pH_i increase could rescue hyperactivation following mSEMG1 treatment. Our findings showed that hyperactivated motility remained suppressed despite pH_i alkalization, indicating a downstream effect or direct binding to CatSper. It is worth noting that $[Ca^{2+}]_i$ increase during capacitation contributes to Em hyperpolarization and intracellular alkalinization, forming a positive feedback loop that in turn potentiates CatSper activity (49, 51). In this regard, Em hyperpolarization is mediated by KSper, which localizes along the sperm flagellum (45, 52). mSEMG1 did not alter Em hyperpolarization during sperm capacitation, indicating that it does not affect KSper activity. Given the relevance of Em hyperpolarization for acrosome exocytosis, our results highlight the relevance of further investigating the role of SEMG1 on this crucial sperm event in future studies.

Altogether, our observations support the conclusion that SEMG1-mediated CatSper inhibition occurs independently of pH_i or Em changes. Therefore, further studies are needed to determine whether SEMG1 binds directly to CatSper subunits or interferes indirectly with channel activation, secondary to protein-protein interactions or inhibition of specific signaling pathways. One putative mechanism involves the ability of SEMG1 to stabilize membrane microdomains through modulation of cholesterol removal and binding to lipid raft components, such as the ganglioside GM1 (53), which may in turn affect capacitation-associated membrane modifications and modulate CatSper activity. Further experimental evidence is required to test this hypothesis.

Our findings identified two domains within the mSEMG1 Q32-V118 and R98-S220 sequences that play crucial roles in inhibiting sperm hyperactivation. Consistently, truncated constructs containing these sequences promoted inhibition of CatSper activity to a similar extent as the full-length mSEMG1. These findings are consistent with previous observations that SEMG1 is a modular protein, containing distinct domains that independently contribute to its multifunctional roles in sperm function and protection (46). Physiologically, SEMG1 associates with the sperm surface through binding to EPPIN, an event that is crucial for the inhibition of sperm motility in the semen coagulum (25, 29, 34). Our previous results demonstrated the co-immunoprecipitation of EPPIN and SEMG1 from mouse spermatozoa incubated with the seminal vesicle fluid when either anti-EPPIN or anti-SEMG1 antibodies were used, indicating a parallel system to humans (21). Thus, we decided to investigate the relevance of EPPIN binding to the effects of mSEMG1 on sperm function. First, we showed that mouse EPPIN and SEMG1 are binding partners, confirming

that EPPIN is a docking site for SEMG1 on the mouse sperm surface. The functional conservation of EPPIN as a sperm-associated hub for SEMG1 binding in both humans and mice was further demonstrated by the capacity of mouse EPPIN to bind human SEMG1. Moreover, we identified the mSEMG1 R98-S220 sequence, which lacks its unique cysteine residue but encompasses two long amino acid repeats, as containing the major EPPIN binding domain. This result was unexpected, since human SEMG1 relies on amino acid sequences flanking its unique cysteine residue to bind EPPIN and inhibit sperm motility (37). Likely, the rapid adaptive evolution pattern of the human *SEMG1* and mouse *Semg1* genes could play a role in shifting the EPPIN binding site to different pockets in its primary sequence (37). Altogether, our results led us to conclude that mouse SEMG1 may inhibit CatSper and hyperactivation through both EPPIN-dependent and independent mechanisms (e.g., through GM1 binding?).

Based on our findings, we propose a working model by which SEMG1 regulates hyperactivation in ejaculated spermatozoa in mice (Fig. 7). SEMG1 coats the surface of spermatozoa at least in part through EPPIN binding in the semen coagulum/copulatory plug, preventing premature hyperactivation and capacitation within the female reproductive tract. This event is mediated by two distinct SEMG1 domains within Q32-V118 and R98-S220 sequences that independently inhibit CatSper activity. In the oviduct, a putative PSA-like protease (likely belonging to the kallikrein family) cleaves SEMG1, allowing spermatozoa to undergo hyperactivation and capacitation. Collectively, these findings position SEMG1 Q32-V118 and R98-S220 sequences as compelling prototypes for the rational design of CatSper inhibitors with potential applications in male contraception targeting critical regulatory pathways for hyperactivation.

Experimental Procedures

Animals

We used male (90–120 days old) and female (60–90 days old) Swiss mice obtained from the Center for Research and Production of Laboratory Animals (CPPA) of São Paulo State University, Botucatu, SP, Brazil. The animals were maintained under controlled conditions (12 h light/dark cycle, 22–24 °C) with food and water available ad libitum. All procedures were approved by the Animal Care and Use Committee of UNESP (protocol #5219150420) and followed the guidelines of the Brazilian National Council for the Control of Animal Experimentation (CONCEA). We also used wild-type (WT) and CatSper1-deficient male C57BL/6 mice, maintained at the Animal Facility of Washington University in St. Louis, School of Medicine, St. Louis, MO, United States (protocol #22-0251), and the Facultad de Ciencias Bioquímicas y Farmacéuticas de Rosario, Rosario, SF, Argentina (protocol #492/2018). These animals were used for patch-clamp recordings, membrane potential analysis, and additional sperm motility experiments. All experiments were conducted following the institutional guidelines for animal research and were approved by the respective Animal Care and Use Committees. Mice were euthanized by inhaled isoflurane overdose or CO_2 inhalation, followed by cervical dislocation.

Protein-protein interaction assays

We performed AlphaScreen to evaluate protein–protein interactions as described in (37), with the following modifications. Briefly, recombinant mEPPIN and its N-terminal fragment, both containing an N-terminal GST-tag, were pre-incubated with anti-GST acceptor beads for 60 minutes. In parallel, mSEMG1 and its truncated fragments (Fig. 4A), containing a 6x-His tag, were incubated with Ni-NTA-chelate donor beads under the same conditions. Equal volumes of the mEPPIN/acceptor bead suspension and the mSEMG1/donor bead suspension were transferred to white opaque 384-well microplates (OptiPlate-384; PerkinElmer, Waltham, MA), in a final reaction volume of 30 µL per well. Plates were sealed and placed in a Synergy 2 Multiplatform automated plate reader (BioTek, Winooski, VT). After 2 minutes of shaking, readings were taken every 2 hrs over 8 hrs, using a 680/30 excitation filter and a 570/100 emission filter. Data acquisition was performed using Gen5 software (BioTek), and a total of 9 time points were recorded per experiment. All conditions were assayed in triplicate.

Final concentrations of the assay components ranged from 0.1–10 nM for mEPPIN, 0.3–100 nM for mSEMG1, and 10 µg/mL for the donor and acceptor beads. Negative controls were conducted under the same conditions in the absence of either mEPPIN or mSEMG1, with beads only. The specific signal at each time point was calculated by subtracting the background signal (obtained in the absence of one of the proteins) from the total signal. To determine the EC_{50} for mEPPIN binding to mSEMG1, we applied nonlinear regression curve fitting to the specific signal values obtained after 4 hrs of incubation. For competition assays, we incubated mEPPIN (10 nM) and mSEMG1 (30 nM) in the presence of increasing concentrations of anti-EPPIN Q20E (targeting the P20–E39 epitope) or anti-EPPIN S21C (targeting the S103–C121 epitope) antibodies, maintaining a total reaction volume of 30 µL and bead concentration at 10 µg/mL. Specific signals for each competitor concentration were calculated as described, and IC_{50} values were determined by nonlinear regression. The expression and purity of mEPPIN and mSEMG1 were confirmed by Western blot before the experiments (Fig. S4).

Analysis of Sperm Motility

Analysis of sperm motility was performed as described in (30), with the following modifications. We collected mouse spermatozoa from the cauda epididymides and incubated them in human tubal fluid (HTF) medium at 37 °C under 5% CO_2. After 10 min of incubation, we removed the tissue and diluted the sperm suspension (~40,000 cells) in HTF supplemented with 25 mM sodium bicarbonate and 0.75% bovine serum albumin (BSA; Sigma, cat. #SLBT1197). We treated the sperm suspensions with recombinant mSEMG1 or its truncated constructs (1–25 µM) (Fig. 4). Negative controls were prepared using HTF medium without recombinant proteins. Rescue experiments were performed to assess whether intracellular alkalinization could counteract the

inhibitory effects of mSEMG1 on sperm motility. Alkalinization was induced by NH_4Cl addition, and its efficacy was verified by analyzing sperm motility under non-capacitating conditions (medium lacking bicarbonate and BSA) following NH_4Cl treatment. Sperm motility was analyzed using a computer-assisted sperm analysis (CASA) system (Hamilton-Thorne, Beverly, MA, USA) with Animal Motility II Software version 1.9. We acquired images using an Olympus CX41 microscope equipped with a MiniTherm stage warmer and a JAI CM-040 digital camera. Aliquots of the sperm suspensions were loaded into pre-warmed 80-µm 2X-CEL slides (Hamilton-Thorne) at 37 °C using large-bore pipette tips. We assessed sperm motility at 20-120 minutes after incubation.

We recorded sperm tracks for 1.5 s (90 frames) at a frame rate of 60 Hz using a 40× negative-phase contrast objective. For each sample, we analyzed at least 200 spermatozoa across 10 different fields. We used video playback to review and manually correct the tracks, removing mistracked cells caused by collisions or debris interference. We then extracted individual ASCII files containing the kinematic parameters for each sperm cell. The following parameters were analyzed: average path velocity (VAP, mm/s), straight-line velocity (VSL, mm/s), curvilinear velocity (VCL, mm/s), amplitude of lateral head displacement (ALH, µm), straightness (STR, %), and linearity (LIN, %). We classified sperm as progressive when VAP > 50 mm/s and STR > 50%, hyperactivated when VCL > 180 mm/s, ALH > 9.5 µm, and LIN < 23.6%, and slow when VAP ≤ 30 µm/s and VSL ≤ 20 µm/s (30). To assess the potential effects of mSEMG1 and its fragments on sperm viability after the maximum incubation period of 120 min under capacitating conditions, viability was evaluated in parallel with motility assays using eosin-nigrosin staining.

Electrophysiology

Electrophysiological recordings were performed as described in (44). In summary, gigaohm seals were established at the cytoplasmic droplet of mouse sperm (Fig. 3) using HS containing (in mM): 130 NaCl, 5 KCl, 1 $MgSO_4$, 2 $CaCl_2$, 5 glucose, 1 sodium pyruvate, 10 lactic acid, and 20 HEPES (pH 7.4). Whole-cell configuration was achieved by applying brief (1 ms) voltage pulses of 400–630 mV combined with gentle suction. Currents were elicited with voltage ramps from −80 mV to +80 mV, starting from a holding potential of 0 mV, in both HS and divalent-free (DVF) bath solutions. Data were acquired at a sampling rate of 2–5 kHz using a low-pass filter at 1 kHz. Patch pipettes (11–17 MΩ) were filled with an internal solution containing (in mM): 130 Cs-methanesulfonate, 70 HEPES, 3 EGTA, 2 EDTA, and 0.5 Tris-HCl (pH adjusted to 7.4 with CsOH). The DVF bath solution used for recording monovalent CatSper currents contained (in mM): 140 Cs-methanesulfonate, 40 HEPES, and 1 EDTA (pH 7.4, adjusted with CsOH). Baseline (leak) currents were recorded in HS before switching to DVF. To evaluate the effects of mSEMG1 and its fragments, proteins (5 or 10 µM; 400–500 µL) were diluted in DVF and added in real-time during the recordings. The complete compositions of the HS, DVF, and pipette solutions are listed in Tables S1, S2, and S3. All electrophysiology recordings were conducted at Washington University in St. Louis, School of Medicine, St. Louis, MO, USA.

Membrane Potential assays

Changes in sperm Em were assessed using DiSC3(5) (Molecular Probes, cat. #D306), as described in (5). A sperm suspension aliquot (~4.0 x 10 cells) was diluted in TYH medium supplemented with 20 mM sodium bicarbonate and 0.5% bovine serum albumin (BSA, Sigma cat. #SLBT1197), with or without mSEMG1 and its fragments (10 μM). Capacitated and non-capacitated sperm in the absence of mSEMG1 were used as experimental controls. After treatment with the proteins and 30 min of capacitation, cells were stained with the Em-sensitive dye DiSC3(5) 1 μM (Molecular Probes) for 2 min. Spermatozoa were transferred to a cuvette at 37°C with mild agitation, and fluorescence was monitored using a Cary Eclipse fluorescence spectrophotometer (Agilent, CA) at excitation/emission wavelengths of 620/670 nm. Recordings began when steady-state fluorescence was reached, and calibration was performed at the end of each measurement by adding 1 μM valinomycin with sequential KCl additions for internal calibration curves. Sperm Em was derived from initial fluorescence (measured in arbitrary fluorescence units) by linear interpolation of theoretical Em values from the calibration curve against arbitrary fluorescence units for each trace. This internal calibration for each determination compensated for variables influencing absolute fluorescence values.

Statistical Analysis

Data are presented as mean ± SEM. Normality and homoscedasticity were assessed using the Kolmogorov–Smirnov test and F-test, respectively. Statistical differences between two independent groups were analyzed using an unpaired Student's t-test; for comparisons involving more than two groups, one-way ANOVA followed by Dunnett's post hoc test was used. For electrophysiological recordings, a paired Student's t-test was applied. Percentage data were arcsine square root transformed before statistical analysis (54). A p-value < 0.05 was considered statistically significant.

Data availability

All data are available in the main text or the supporting information.

Supporting information

This article contains supporting information.

Acknowledgments

We thank Luiz Oliveira, Paulo Mioni, and Flávia Colenci, Ph.D., Department of Biophysics and Pharmacology, IBB/UNESP, for their technical assistance. We are also grateful to Michael

O´Rand, Ph.D., and Katherine Hamil, M.Sc., for their critical reading of the manuscript and valuable insights, and Célio Fernandes, Ph.D., for his helpful discussions during the project.

Author contributions

Mariani NAP and Silva EJR: conceptualization; Mariani NAP, Steeman TJ, Novero AG, Lima JC, Krapf D, Lishko P, Silva EJR: methodology; Mariani NAP, Santos NCM and Silva EJR: formal analysis; Mariani NAP, Santos NCM, Andrade AD, Rezende B, Andrade JJ, Steeman TJ, Novero AG, Calderaro G, Themer ACF, Kushima H: investigation; Mariani NAP, Santos NCM, Andrade AD, and Silva EJR: visualization; Silva EJR, Lishko PV, and Krapf D: resources; Silva EJR: funding acquisition; Mariani NAP and Silva EJR: writing-original draft; Mariani NAP, Santos NCM, Andrade AD, Rezende B, Lishko PV, Krapf D, Buffone MG, and Silva EJR: writing–review & editing; Silva EJR, Lishko PV, Krapf D and Buffone MG: supervision. All authors have read and agree with the final version of the manuscript.

Funding and additional information

This study was funded by São Paulo Research Foundation (FAPESP, grants 2020/04841-3, 2021/04746-3, 2021/06718-7, 2022/10159-6, 2023/00125-0, and 2023/04496-2), Coordenação de Aperfeiçoamento de Pessoal de Nível Superior (CAPES, grants 88887.496465/2020-00 and 88887.657625/2021-00), Conselho Nacional de Desenvolvimento Científico e Tecnológico (CNPq, grants 303616/2022-9, 442218/2023-0, and 201112/2024-8), Fondo para la Investigación Científica y Tecnológica (2021-1-0102) to Krapf D, and Barnes Jewish Hospital Foundation St. Louis (BJC) grant to Lishko PV.

Conflict of Interest

The authors declare that they have no conflict of interest.

References

1. Freitas, M. J., Vijayaraghavan, S., and Fardilha, M. (2017) Signaling mechanisms in mammalian sperm motility. *Biol. Reprod.* **96**, 2–12

2. Stival, C., Puga Molina, L. del C., Paudel, B., Buffone, M. G., Visconti, P. E., and Krapf, D. (2016) Sperm capacitation and acrosome reaction in mammalian sperm. *Adv. Anat. Embryol. Cell Biol.* **220**, 93–106

3. Austin, C. R. (1952) The ‘capacitation’ of the mammalian sperm. *Nature*. **170**, 326–326

4. Vyklicka, L., and Lishko, P. V. (2020) Dissecting the signaling pathways involved in the function of sperm flagellum. *Curr. Opin. Cell Biol.* **63**, 154–161

5. Ritagliati, C., Baro Graf, C., Stival, C., and Krapf, D. (2018) Regulation mechanisms and implications of sperm membrane hyperpolarization. *Mech. Dev.* **154**, 33–43

6. Witte, T. S., and Schäfer-Somi, S. (2007) Involvement of cholesterol, calcium and progesterone in the induction of capacitation and acrosome reaction of mammalian spermatozoa. *Anim. Reprod. Sci.* **102**, 181–193

7. Visconti, P. E., Westbrook, V. A., Chertihin, O., Demarco, I., Sleight, S., and Diekman, A. B. (2002) Novel signaling pathways involved in sperm acquisition of fertilizing capacity. *J. Reprod. Immunol.* **53**, 133–150

8. López-González, I., Torres-Rodríguez, P., Sánchez-Carranza, O., Solís-López, A., Santi, C. M., Darszon, A., and Treviño, C. L. (2014) Membrane hyperpolarization during human sperm capacitation. *Mol. Hum. Reprod.* **20**, 619–629

9. Darszon, A., Nishigaki, T., Beltran, C., and Treviño, C. L. (2011) Calcium channels in the development, maturation, and function of spermatozoa. *Physiol. Rev.* **91**, 1305–1355

10. Lishko, P. V., and Mannowetz, N. (2018) CatSper: a unique calcium channel of the sperm flagellum. *Curr. Opin. Physiol.* **2**, 109–113

11. Hwang, J. Y., Mannowetz, N., Zhang, Y., Everley, R. A., Gygi, S. P., Bewersdorf, J., Lishko, P. V., and Chung, J.-J. (2019) Dual sensing of physiologic pH and calcium by EFCAB9 regulates sperm motility. *Cell*. **177**, 1480-1494.e19

12. Lin, S., Ke, M., Zhang, Y., Yan, Z., and Wu, J. (2021) Structure of a mammalian sperm cation channel complex. *Nature*. **595**, 746–750

13. Bystroff, C. (2018) Intramembranal disulfide cross-linking elucidates the super-quaternary structure of mammalian CatSpers. *Reprod. Biol.* **18**, 76–82

14. Zhao, Y., Wang, H., Wiesehoefer, C., Shah, N. B., Reetz, E., Hwang, J. Y., Huang, X., Wang, T., Lishko, P. V., Davies, K. M., Wennemuth, G., Nicastro, D., and Chung, J.-J. (2022) 3D structure and in situ arrangements of CatSper channel in the sperm flagellum. *Nat. Commun.* **13**, 3439

15. Avenarius, M. R., Hildebrand, M. S., Zhang, Y., Meyer, N. C., Smith, L. L. H., Kahrizi, K., Najmabadi, H., and Smith, R. J. H. (2009) Human male infertility caused by mutations in the $CATSPER_1$ channel protein. *Am. J. Hum. Genet.* **84**, 505–510

16. Carlson, A. E., Quill, T. A., Westenbroek, R. E., Schuh, S. M., Hille, B., and Babcock, D. F. (2005) Identical phenotypes of CatSper1 and CatSper2 null sperm. *J. Biol. Chem.* **280**, 32238–32244

17. Chung, J.-J., Miki, K., Kim, D., Shim, S.-H., Shi, H. F., Hwang, J. Y., Cai, X., Iseri, Y., Zhuang, X., and Clapham, D. E. (2017) CatSperζ regulates the structural continuity of sperm Ca^{2+} signaling domains and is required for normal fertility. *eLife*. **6**, e23082

18. Hildebrand, M. S., Avenarius, M. R., Fellous, M., Zhang, Y., Meyer, N. C., Auer, J., Serres, C., Kahrizi, K., Najmabadi, H., Beckmann, J. S., and Smith, R. J. H. (2010) Genetic male infertility and mutation of CATSPER ion channels. *Eur. J. Hum. Genet. EJHG*. **18**, 1178–1184

19. De Jonge, C. (2005) Biological basis for human capacitation. *Hum. Reprod. Update*. **11**, 205–214

20. Chang, M. C. (1951) Fertilizing capacity of spermatozoa deposited into the fallopian tubes. *Nature*. **168**, 697–698

21. Mariani, N. A. P., Camara, A. C., Silva, A. A. S., Raimundo, T. R. F., Andrade, J. J., Andrade, A. D., Rossini, B. C., Marino, C. L., Kushima, H., Santos, L. D., and Silva, E. J. R. (2020) Epididymal protease inhibitor (EPPIN) is a protein hub for seminal vesicle-secreted protein SVS2 binding in mouse spermatozoa. *Mol. Cell. Endocrinol.* **506**, 110754

22. Silva, E. J. R., Hamil, K. G., Richardson, R. T., and O'Rand, M. G. (2012) Characterization of EPPIN's semenogelin I binding site: a contraceptive drug target. *Biol. Reprod.* **87**, 56

23. Wang, Z., Widgren, E. E., Sivashanmugam, P., O'Rand, M. G., and Richardson, R. T. (2005) Association of eppin with semenogelin on human spermatozoa. *Biol. Reprod.* **72**, 1064–1070

24. Wang, Z., Widgren, E. E., Richardson, R. T., and O'Rand, M. G. (2007) Characterization of an Eppin protein complex from human semen and spermatozoa. *Biol. Reprod.* **77**, 476–484

25. Mitra, A., Richardson, R. T., and O'Rand, M. G. (2010) Analysis of recombinant human semenogelin as an inhibitor of human sperm motility. *Biol. Reprod.* **82**, 489–496

26. Kawano, N., and Yoshida, M. (2007) Semen-coagulating protein, SVS2, in mouse seminal plasma controls sperm fertility. *Biol. Reprod.* **76**, 353–361

27. Araki, N., Kawano, N., Kang, W., Miyado, K., Yoshida, K., and Yoshida, M. (2016) Seminal vesicle proteins SVS3 and SVS4 facilitate SVS2 effect on sperm capacitation. *Reproduction*. 10.1530/REP-15-0551

28. Sakaguchi, D., Miyado, K., Iwamoto, T., Okada, H., Yoshida, K., Kang, W., Suzuki, M., Yoshida, M., and Kawano, N. (2020) Human semenogelin 1 promotes sperm survival in the mouse female reproductive tract. *Int. J. Mol. Sci.* **21**, 3961

29. O'Rand, M. G., Widgren, E. E., Beyler, S., and Richardson, R. T. (2009) Inhibition of human sperm motility by contraceptive anti-eppin antibodies from infertile male monkeys: effect on cyclic adenosine monophosphate. *Biol. Reprod.* **80**, 279–285

30. Silva, A. A. S., Raimundo, T. R. F., Mariani, N. A. P., Kushima, H., Avellar, M. C. W., Buffone, M. G., Paula-Lopes, F. F., Moura, M. T., and Silva, E. J. R. (2021) Dissecting EPPIN protease inhibitor domains in sperm motility and fertilizing ability: repercussions for male contraceptive development. *Mol. Hum. Reprod.* **27**, gaab066

31. O'Rand, M. G., Hamil, K. G., Adevai, T., and Zelinski, M. (2018) Inhibition of sperm motility in male macaques with EP055, a potential non-hormonal male contraceptive. *PloS One*. **13**, e0195953

32. Robert, M., and Gagnon, C. (1999) Semenogelin I: a coagulum forming, multifunctional seminal vesicle protein. *Cell. Mol. Life Sci. CMLS*. **55**, 944–960

33. Kawano, N., Araki, N., Yoshida, K., Hibino, T., Ohnami, N., Makino, M., Kanai, S., Hasuwa, H., Yoshida, M., Miyado, K., and Umezawa, A. (2014) Seminal vesicle protein SVS2 is required for sperm survival in the uterus. *Proc. Natl. Acad. Sci. U. S. A.* **111**, 4145–4150

34. O'Rand, M. G., and Widgren, E. E. (2012) Loss of calcium in human spermatozoa via EPPIN, the semenogelin receptor. *Biol. Reprod.* **86**, 55

35. Katz, D. F., and Vanagimachi, R. (1980) Movement characteristics of hamster spermatozoa within the oviduct. *Biol. Reprod.* **22**, 759–764

36. Suarez, S. S. (1987) Sperm transport and motility in the mouse oviduct: observations in situ. *Biol. Reprod.* **36**, 203–210

37. Silva, E. J. R., Hamil, K. G., and O'Rand, M. G. (2013) Interacting proteins on human spermatozoa: adaptive evolution of the binding of semenogelin I to EPPIN. *PLoS ONE*. **8**, e82014

38. Cancel, A. M., Lobdell, D., Mendola, P., and Perreault, S. D. (2000) Objective evaluation of hyperactivated motility in rat spermatozoa using computer-assisted sperm analysis. *Hum. Reprod.* **15**, 1322–1328

39. Kirichok, Y., Navarro, B., and Clapham, D. E. (2006) Whole-cell patch-clamp measurements of spermatozoa reveal an alkaline-activated Ca2+ channel. *Nature*. **439**, 737–740

40. Ren, D., Navarro, B., Perez, G., Jackson, A. C., Hsu, S., Shi, Q., Tilly, J. L., and Clapham, D. E. (2001) A sperm ion channel required for sperm motility and male fertility. *Nature*. **413**, 603–609

41. Quill, T. A., Sugden, S. A., Rossi, K. L., Doolittle, L. K., Hammer, R. E., and Garbers, D. L. (2003) Hyperactivated sperm motility driven by CatSper2 is required for fertilization. *Proc. Natl. Acad. Sci. U. S. A.* **100**, 14869–14874

42. Young, S., Schiffer, C., Wagner, A., Patz, J., Potapenko, A., Herrmann, L., Nordhoff, V., Pock, T., Krallmann, C., Stallmeyer, B., Röpke, A., Kierzek, M., Biagioni, C., Wang, T., Haalck, L., Deuster, D., Hansen, J. N., Wachten, D., Risse, B., Behre, H. M., Schlatt, S., Kliesch, S., Tüttelmann, F., Brenker, C., and Strünker, T. (2024) Human fertilization in vivo and in vitro requires the CatSper channel to initiate sperm hyperactivation. *J. Clin. Invest.* **134**, e173564

43. Kirichok, Y., and Lishko, P. V. (2011) Rediscovering sperm ion channels with the patch-clamp technique. *Mol. Hum. Reprod.* **17**, 478–499

44. Liu, B., Mundt, N., Miller, M., Clapham, D. E., Kirichok, Y., and Lishko, P. V. (2021) Recording electrical currents across the plasma membrane of mammalian sperm cells. *J. Vis. Exp. JoVE*. 10.3791/62049

45. Mannowetz, N., Naidoo, N. M., Choo, S.-A. S., Smith, J. F., and Lishko, P. V. (2013) Slo1 is the principal potassium channel of human spermatozoa. *eLife*. **2**, e01009

46. de Lamirande, E., and Lamothe, G. (2010) Levels of semenogelin in human spermatozoa decrease during capacitation: involvement of reactive oxygen species and zinc. *Hum. Reprod. Oxf. Engl.* **25**, 1619–1630

47. Araki, N., Trencsényi, G., Krasznai, Z. T., Nizsalóczki, E., Sakamoto, A., Kawano, N., Miyado, K., Yoshida, K., and Yoshida, M. (2015) Seminal vesicle secretion 2 acts as a protectant of sperm sterols and prevents ectopic sperm capacitation in mice. *Biol. Reprod.* **92**, 8

48. Wang, D., Hu, J., Bobulescu, I. A., Quill, T. A., McLeroy, P., Moe, O. W., and Garbers, D. L. (2007) A sperm-specific Na^+/H^+ exchanger (sNHE) is critical for expression and in vivo bicarbonate regulation of the soluble adenylyl cyclase (sAC). *Proc. Natl. Acad. Sci. U. S. A.* **104**, 9325–9330

49. Novero, A. G., Torres Rodríguez, P., De la Vega Beltrán, J. L., Schiavi-Ehrenhaus, L. J., Luque, G. M., Carruba, M., Stival, C., Gentile, I., Ritagliati, C., Santi, C. M., Nishigaki, T., Krapf, D., Buffone, M. G., Darszon, A., Treviño, C. L., and Krapf, D. (2024) The sodium-proton exchangers sNHE and NHE1 control plasma membrane hyperpolarization in mouse sperm. *J. Biol. Chem.* **300**, 107932

50. Wang, H., McGoldrick, L. L., and Chung, J.-J. (2021) Sperm ion channels and transporters in male fertility and infertility. *Nat. Rev. Urol.* **18**, 46–66

51. Chávez, J. C., Ferreira, J. J., Butler, A., De La Vega Beltrán, J. L., Treviño, C. L., Darszon, A., Salkoff, L., and Santi, C. M. (2014) SLO3 K+ channels control calcium entry through CATSPER channels in sperm. *J. Biol. Chem.* **289**, 32266–32275

52. Navarro, B., Kirichok, Y., and Clapham, D. E. (2007) KSper, a pH-sensitive K+ current that controls sperm membrane potential. *Proc. Natl. Acad. Sci. U. S. A.* **104**, 7688–7692

53. Kawano, N., Yoshida, K., Iwamoto, T., and Yoshida, M. (2008) Ganglioside GM1 mediates decapacitation effects of SVS2 on murine spermatozoa. *Biol. Reprod.* **79**, 1153–1159

54. Zar, J. H. (2010) *Biostatistical Analysis*, 5th edition, Pearson Prentice Hall, New Jersey

Figure Legends

Figure 1. Effects of mSEMG1 on murine sperm motility and viability. *A* and *B,* Percentage of total and slow motility of spermatozoa after incubation with mSEMG1. *C,* Percentage of viable spermatozoa after incubation with mSEMG1. Spermatozoa were incubated in capacitating HTF medium in the absence (control) or presence of increasing concentrations of mSEMG1 (1, 3, 10, and 25 µM). Sperm motility was assessed after 20 and 120 min of capacitation, while sperm viability was assessed after 120 min. Dots with the same color represent the values from an independent experiment. Asterisks indicate statistically significant differences from the control group ($p<0.05$, ANOVA followed by Dunnett´s test). Percentage data were transformed using arcsine square-root values before statistical analysis. Results are presented as mean ± SEM values from independent experiments using sperm samples from 3-7 mice.

Figure 2. Effects of mSEMG1 on hyperactivated motility. *A,* Percentage of hyperactivated motility of spermatozoa after incubation with mSEMG1. *B,* Concentration-response curve of hyperactivated motility rate of spermatozoa after incubation with mSEMG1. Data were expressed as mean percentage values relative to the control group. Inhibitory concentration 50% (IC_{50}, 95% confidence interval) is presented. *C,* Curvilinear velocity (VCL) (left) and amplitude of lateral head displacement (ALH) (right) of spermatozoa after incubation with mSEMG1. Spermatozoa were isolated from the cauda epididymidis and incubated in capacitating HTF medium in the absence (control) or presence of increasing concentrations of mSEMG1 (1, 3, 10, and 25 µM). *D,* Percentage of hyperactivated spermatozoa in the presence or absence of NH_4Cl. Cells were incubated in non-capacitating medium (Non-Cap), supplemented or not with NH_4Cl (left), or in capacitating medium (Cap), supplemented or not with NH_4Cl in the absence or presence of 10 µM mSEMG1 (right). Sperm motility was assessed after 30 and 120 min of capacitation. Dots with the same color represent the values from an independent experiment. Asterisks indicate statistically significant differences from the control group ($p<0.05$, ANOVA followed by Dunnett´s test). Percentage data were transformed using arcsine square-root values before statistical analysis. Results are presented as mean ± SEM values from independent experiments using sperm samples from 3-6 mice.

Figure 3. Effects of mSEMG1 on $I_{CatSper}$. *A,* Representative DIC image of murine spermatozoon with cytoplasmic droplet (yellow circle) used for patch-clamp recording. Right: Cs^+ concentration and pH of the pipette and bath solutions are indicated. Voltage ramps (-80 mV to 80 mV, 1 s) were applied in HS and in DVF to record $I_{CatSper}$. Baseline currents were recorded in HS (black), which lacked $I_{CatSper}$ due to its inhibition by extracellular magnesium. *B,* Left: $I_{CatSper}$ recordings in response to voltage ramps in DVF before (control) (red) and after addition of 5 µM mSEMG1 (blue), including washout (grey), and recorded from wild-type and CatSper KO (inset) spermatozoa. Traces represent recordings from the same spermatozoon. Right: $I_{CatSper}$ recordings (mean ± SEM;

pA) obtained at −80 mV in DVF solution before and after exposure to 5 μM mSEMG1. $I_{CatSper}$ recording was repeated in DVF after mSEMG1 was washed out. Sperm cell capacitance ranged from 2.0 to 2.6 pF. Dots with the same color represent current values from the same cell. *C,* Current-voltage (I-V) relationships were calculated from amplitudes shown in panel A in the DVF solution before and after 5 μM mSEMG1 treatment. *D,* Quantification of membrane potential (Em) in non-capacitated, capacitated, and capacitated spermatozoa treated with 10 μM mSEMG1. Membrane potential was assessed after 30 min of capacitation. Dots with the same color represent values from independent experiments. Asterisks indicate statistically significant differences from the control group ($p < 0.05$, ANOVA followed by Dunnett's test or paired t-test). Results are presented as mean ± SEM from independent experiments using sperm samples from 3-4 mice.

Figure 4. Mouse SEMG1 sequence, recombinant constructs, and their effects on sperm motility. *A,* Left: Amino acid sequence of mouse SEMG1. The signal peptide is shown in lowercase letters. Amino acid repeats are indicated in bold. The GGS region is underlined, while the KS region and the single cysteine residue are highlighted in red and yellow, respectively. Right: Schematic representation of mSEMG1 full-length and truncated constructs used in the experiments. The mSEMG1 constructs include a 6x-His tag. *B,* Percentage of total motile (left) and hyperactivated (right) spermatozoa after incubation with mSEMG1. *C,* Curvilinear velocity (VCL) (left) and amplitude of lateral head displacement (ALH) (right) of spermatozoa after incubation with mSEMG1 constructs. Spermatozoa were isolated from the cauda epididymidis and incubated in capacitating HTF medium in the absence (control) or presence of mSEMG1 constructs (25 μM). Sperm motility was assessed after 120 min. Dots with the same color represent the values from an independent experiment. Asterisks indicate statistically significant differences from the control group ($p<0.05$, ANOVA followed by Dunnett´s test). Percentage data were transformed using arcsine square-root values before statistical analysis. Results are presented as mean ± SEM values from independent experiments using sperm samples from 3-5 mice.

Figure 5. Effects of mSEMG1 fragments on $I_{CatSper}$. *A-C,* Left: Representative $I_{CatSper}$ recordings in response to voltage ramps in DVF (control) before (red) and after 5 μM $mSEMG1^{Q32–V118}$ (pink), $mSEMG1^{R98–G375}$ (green), and $mSEMG1^{Y221–G375}$ (orange), recorded from wild-type mouse spermatozoa. Baseline currents are recorded in HS (black). Traces represent recordings from the same spermatozoon. Right: Quantification of $I_{CatSper}$ (mean ± SEM; pA) at −80 mV in DVF solution before and after addition of the respective mSEMG1 fragments. Sperm cell capacitance ranged from 2.1 to 2.8 pF. Dots with the same color represent values from independent experiments. Asterisks indicate statistically significant differences from the control group ($p < 0.05$, paired t-test). Results are presented as mean ± SEM from independent experiments using sperm samples from 4-7 mice.

Figure 6. Characterization of the interaction between mSEMG1 and mEPPIN. *A,* Schematic representation of the AlphaScreen assay. GST-tagged mEPPIN was captured by anti-GST acceptor beads, and 6×His-tagged mSEMG1 by Ni^{2+}-chelate donor beads. Upon excitation at 680 nm, a luminescent signal was generated due to the proximity (<200 nm) of donor and acceptor beads, indicating an interaction between mEPPIN and mSEMG1. *B,* mEPPIN was incubated with mSEMG1 in a time-course experiment. Background signal was detected when beads were incubated in the absence of mEPPIN or mSEMG1. Data are presented as mean ± SEM from a representative experiment out of ten, each performed in triplicate. *C,* Left: Concentration-response curve for mSEMG1 with a constant concentration of mEPPIN (10 nM). Right: Concentration-response curve for mEPPIN with a constant concentration of mSEMG1 (30 nM). A specific signal for each data point was determined by subtracting the background signal from the total signal. Results represent mean ± SEM of specific signals from 2-4 experiments. *D,* Left: mSEMG1 and its fragments (Q32-V118: $mSEMG1^{Q32-V118}$, R98-G375: $mSEMG1^{R98-G375}$, and Y221-G375: $SEMG^{Y221-G375}$) were incubated with mEPPIN for 4 hours. Right: mEPPIN and its N-terminal construct (L24-K68: $mEPPIN^{L24-K68}$) were incubated with mSEMG1 for 4 hours. Dots with the same color represent values from independent experiments. Specific signals for each data point were normalized as a percentage of the signal from full-length mSEMG1/mEPPIN binding. Asterisks indicate statistically significant differences from the control group (mSEMG1 or mEPPIN) ($p<0.05$, ANOVA followed by Dunnett´s test). Results are expressed as mean ± SEM of specific signals from 4-10 experiments. Cps = counts per second.

Figure 7. Working model of SEMG1-mediated inhibition of sperm hyperactivation after sperm ejaculation. EPPIN is present on the surface of mature spermatozoa stored in the cauda epididymidis. In the semen coagulum/copulatory plug (Phase 1), SEMG1 binds to the sperm surface via interaction with EPPIN through a binding domain within residues R98-S220, thus coating spermatozoa. SEMG1 may also interact with spermatozoa independently of EPPIN binding. Domains within the SEMG1 Q32-G375 and R98-S220 regions inhibit sperm function, i.e., temporarily preventing hyperactivation in the uterus by inhibiting CatSper, while only the R98-S220 domain contains the EPPIN binding site. As spermatozoa move to the upper regions of the female reproductive tract, SEMG1 is proteolytically cleaved by a PSA-like enzyme (Phase 2), whose identity remains unknown in mice, allowing hyperactivation to take place in the oviduct.

A

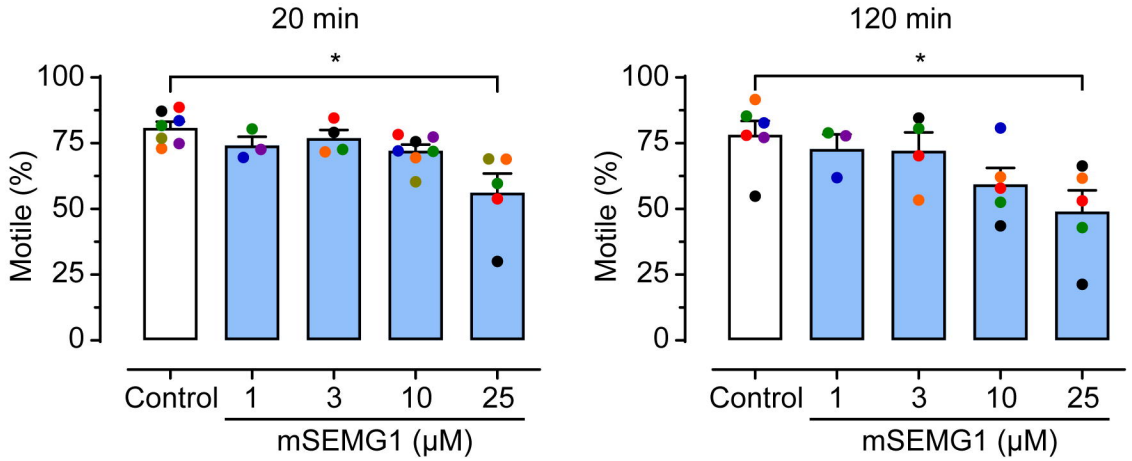
20 min
120 min
Motile (%)
100
75
50
25
0
*
Control
1
3
10
25
mSEMG1 (μM)

B

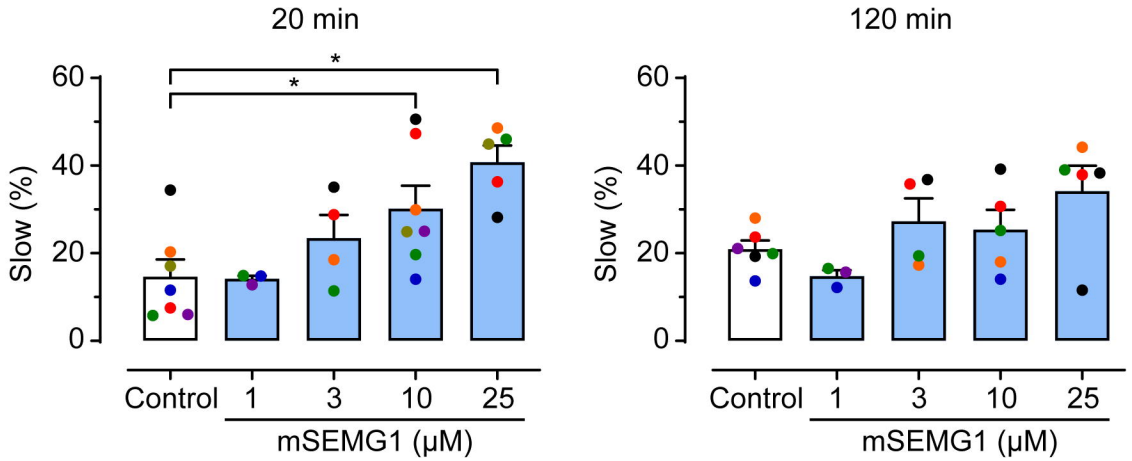
20 min
120 min
Slow (%)
60
40
20
0
*
*
Control
1
3
10
25
mSEMG1 (μM)

C

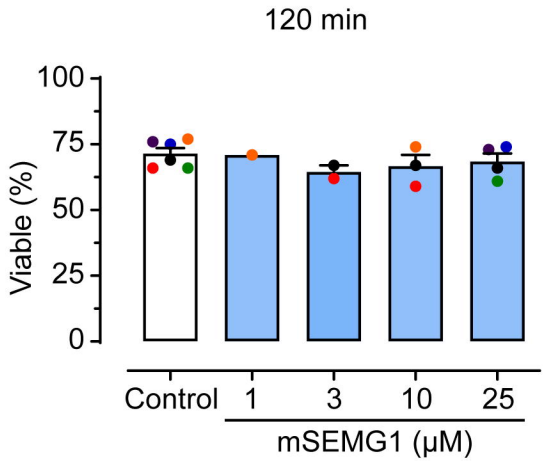
120 min
Viable (%)
100
75
50
25
0
Control
1
3
10
25
mSEMG1 (μM)

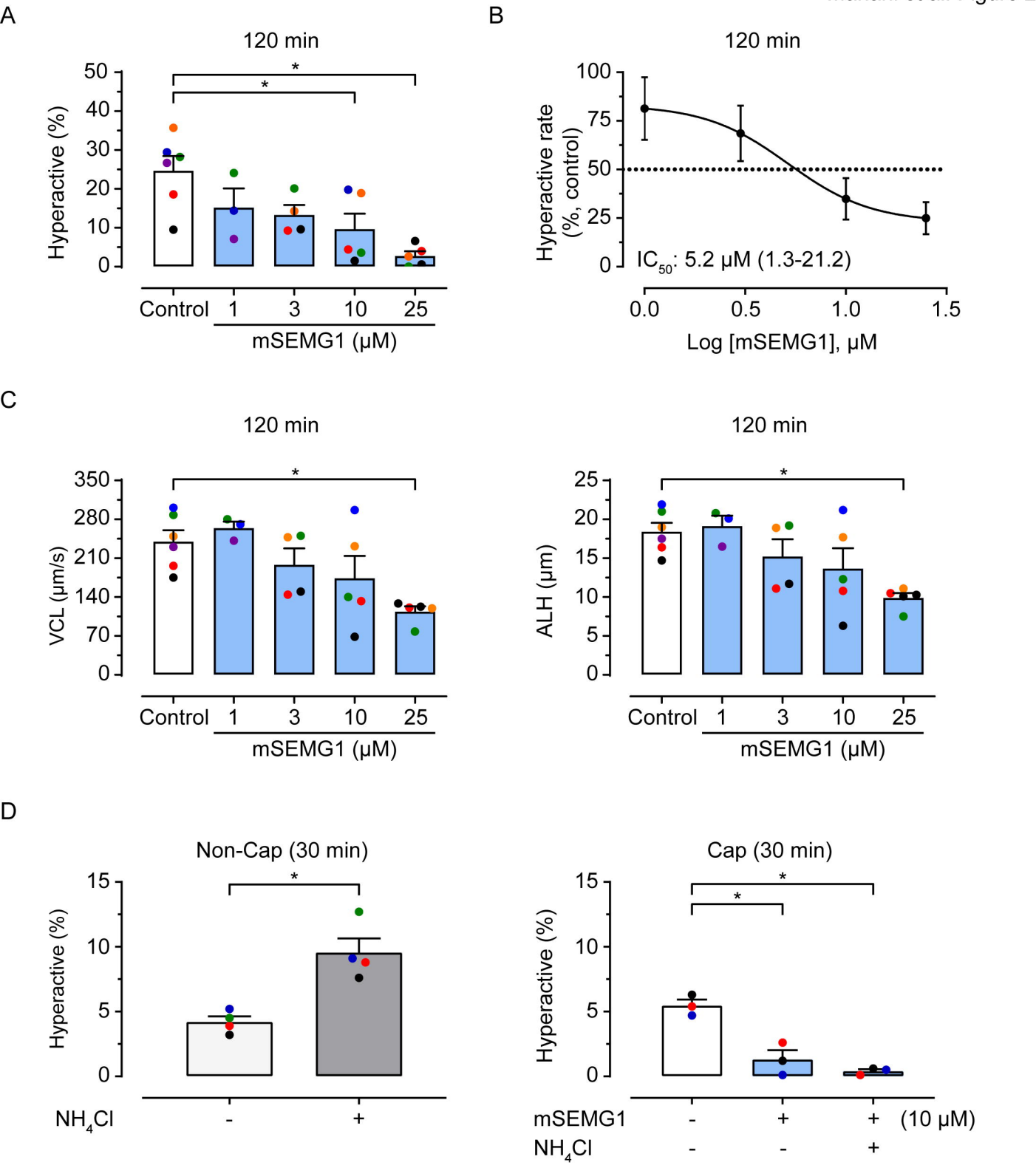
A
120 min
Hyperactive (%)
50
40
30
20
10
0
*
*
Control
1
3
10
25
mSEMG1 (μM)
B
120 min
Hyperactive rate (%, control)
100
75
50
25
0
IC50: 5.2 μM (1.3-21.2)
0.0
0.5
1.0
1.5
Log [mSEMG1], μM
C
120 min
VCL (μm/s)
350
280
210
140
70
0
*
Control
1
3
10
25
mSEMG1 (μM)
120 min
ALH (μm)
25
20
15
10
5
0
*
Control
1
3
10
25
mSEMG1 (μM)
D
Non-Cap (30 min)
Hyperactive (%)
15
10
5
0
*
NH4Cl
-
+
Cap (30 min)
Hyperactive (%)
15
10
5
0
*
*
mSEMG1
-
+
+
(10 μM)
NH4Cl
-
-
+

A

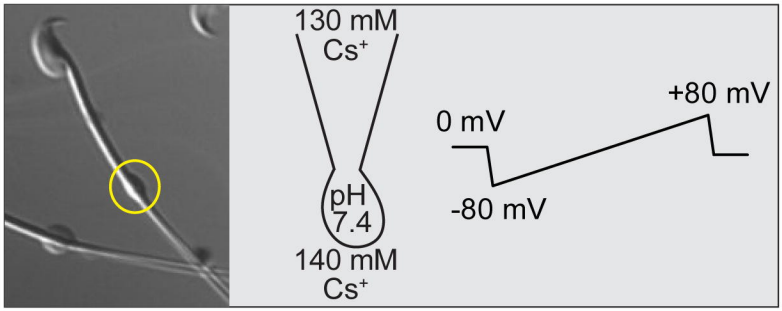
130 mM
Cs+
pH
7.4
140 mM
Cs+
0 mV
-80 mV
+80 mV

B

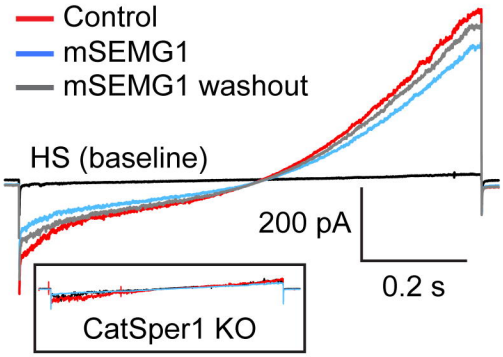
Control
mSEMG1
mSEMG1 washout
HS (baseline)
200 pA
0.2 s
CatSper1 KO

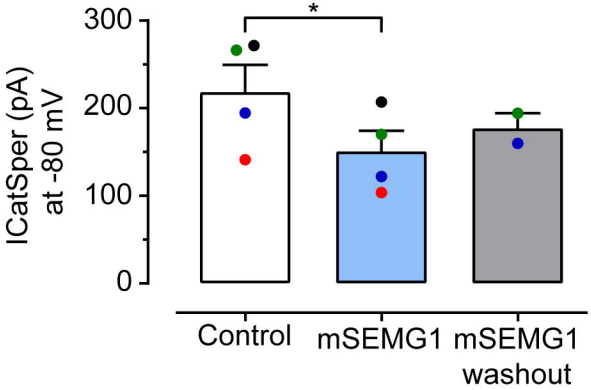
ICatSper (pA)
at -80 mV
300
200
100
0
*
Control
mSEMG1
mSEMG1
washout

C

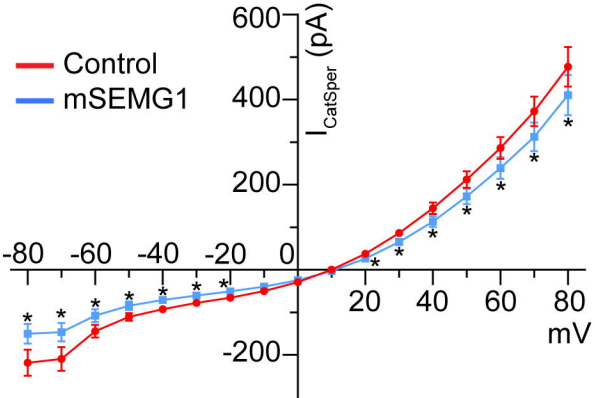
Control
mSEMG1
I CatSper (pA)
600
400
200
-200
-80
-60
-40
-20
0
20
40
60
80
mV

D

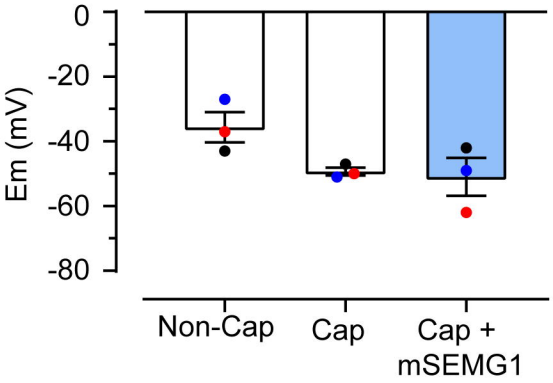
Em (mV)
0
-20
-40
-60
-80
Non-Cap
Cap
Cap +
mSEMG1

A

SEMG1 (*Mus musculus*, NP_059086)

```
1...................20...................40...................60
mkssvfvlslllilerqsavvgQYGATKGNFQSSSSEGFMLGQKGRLSFGIKGGSDEAAE
61..................80...................100..................120
ESLFMQSQRRVYGQGGGDMTQTRVSQEHTSVKGAAILCRNGQVSQLKSQESQIKSYGQVKS
121.................140..................160..................180
SGQLKSGGSAFGQVKSSVSQIKSYGQLKSGGQLKSGGPAFGQVKSQESQIKSYGQLKSSG
181.................200..................220..................240
QLKSGGSAFGQVKSSVSQIKSYGQLKSGGSQVKSYGQTKSYGEEGQLNSFSQLKSQGAQL
241.................260..................280..................300
KSYGQQKSQQQSSFSQVKSQSSQLKSYGQQKSLKGFSQQTQHKGFAMDEGMSQVRKQFSD
301.................320..................340..................360
DDLSVQQKSTQQMKTEEDLSQFGQQRQYGQERSQSYKGYLEQYRKKVQEQQRKNFNPGNY
361...........375
FTKGGADLYQAQLKG
```

Recombinant mouse SEMG1 constructs

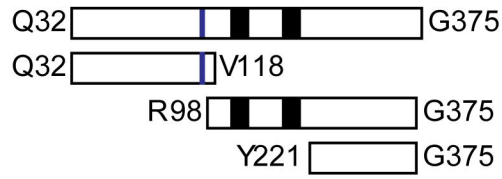

B

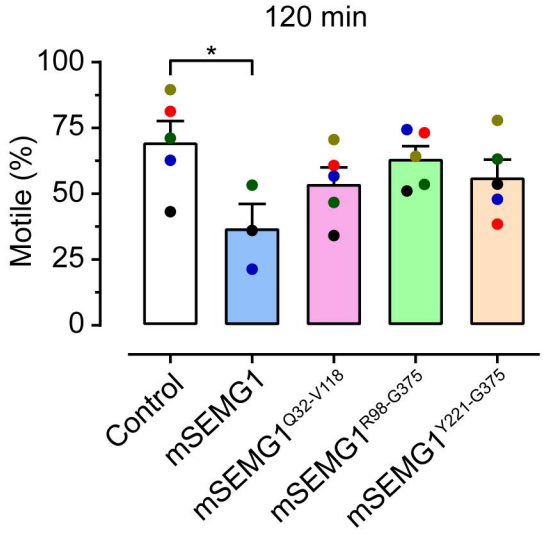

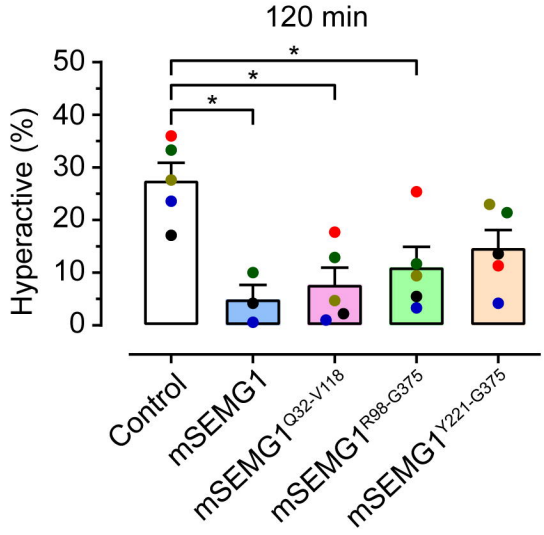

C

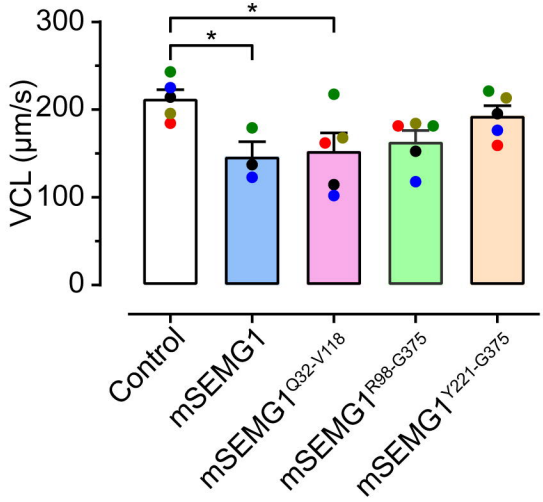

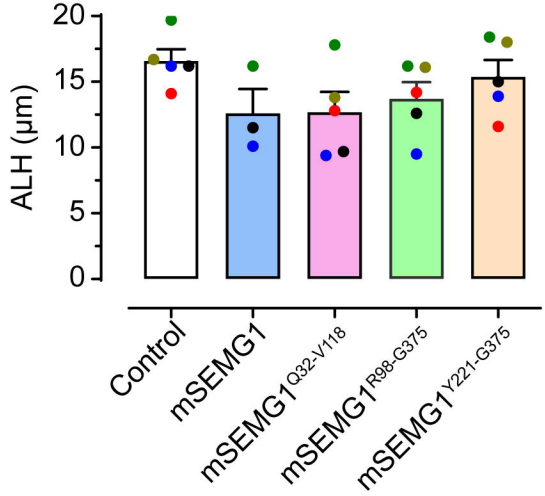

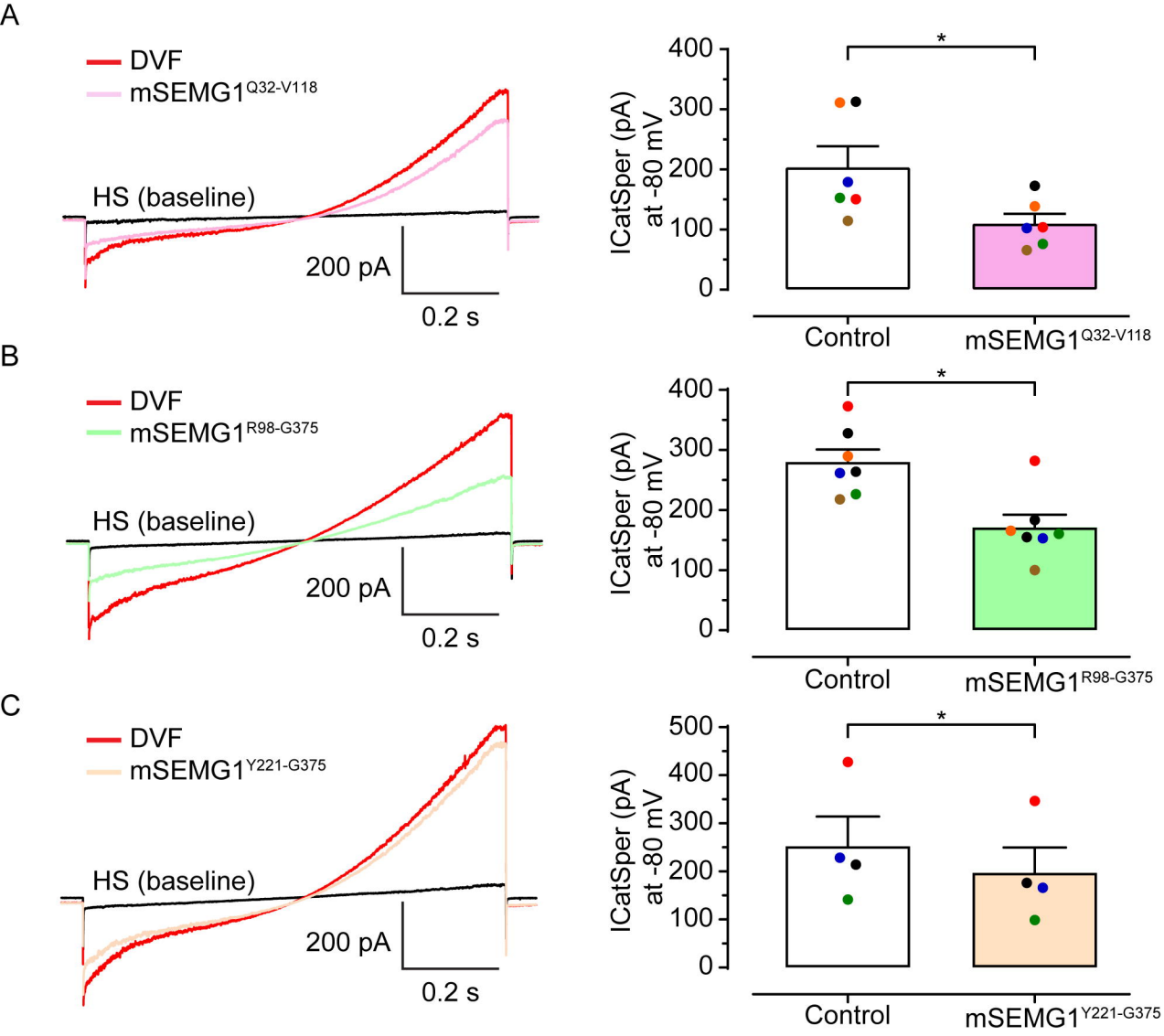
A
DVF
mSEMG1Q32-V118
HS (baseline)
200 pA
0.2 s
ICatSper (pA) at -80 mV
400
300
200
100
0
*
Control
mSEMG1Q32-V118
B
DVF
mSEMG1R98-G375
HS (baseline)
200 pA
0.2 s
ICatSper (pA) at -80 mV
400
300
200
100
0
*
Control
mSEMG1R98-G375
C
DVF
mSEMG1Y221-G375
HS (baseline)
200 pA
0.2 s
ICatSper (pA) at -80 mV
500
400
300
200
100
0
*
Control
mSEMG1Y221-G375

A

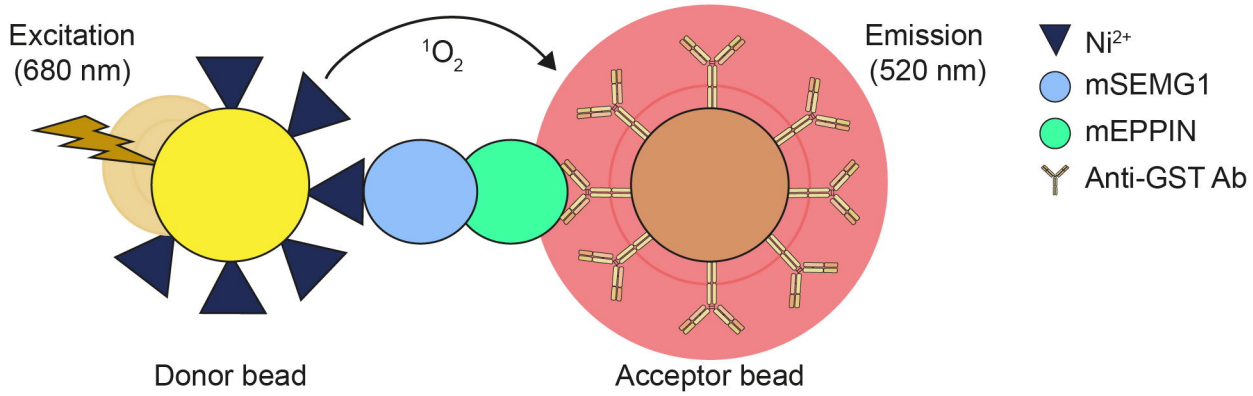
Excitation
(680 nm)
$^1O_2$
Emission
(520 nm)
Ni^{2+}
mSEMG1
mEPPIN
Anti-GST Ab
Donor bead
Acceptor bead

B

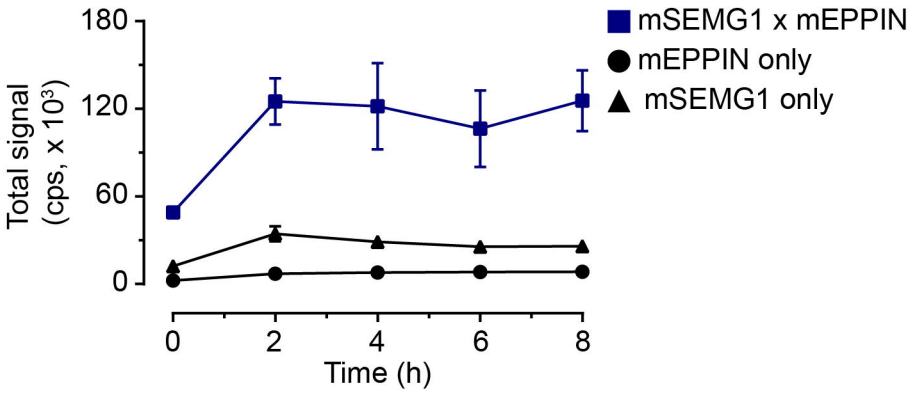
mSEMG1 x mEPPIN
mEPPIN only
mSEMG1 only
Total signal
(cps, x 10^3)
180
120
60
0
0
2
4
6
8
Time (h)

C

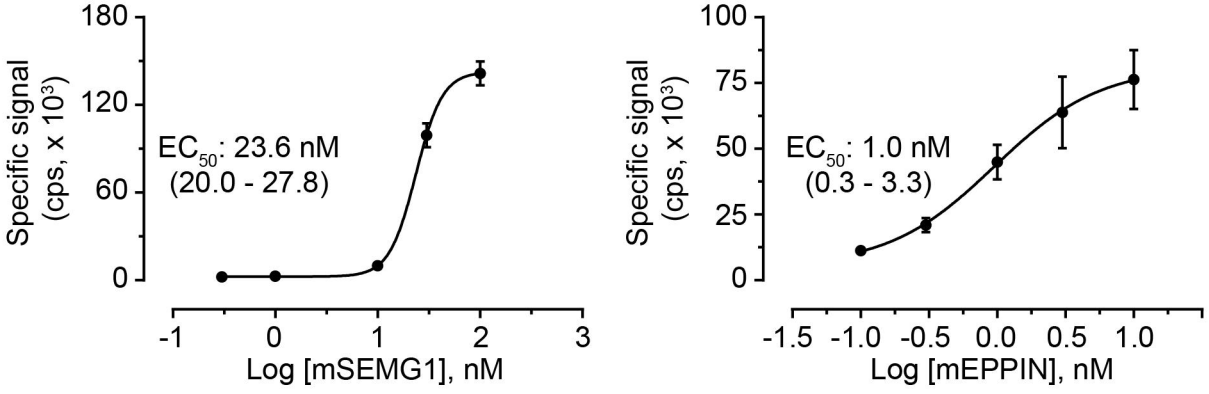
Specific signal
(cps, x 10^3)
EC_{50}: 23.6 nM
(20.0 - 27.8)
Log [mSEMG1], nM
Specific signal
(cps, x 10^3)
EC_{50}: 1.0 nM
(0.3 - 3.3)
Log [mEPPIN], nM

D

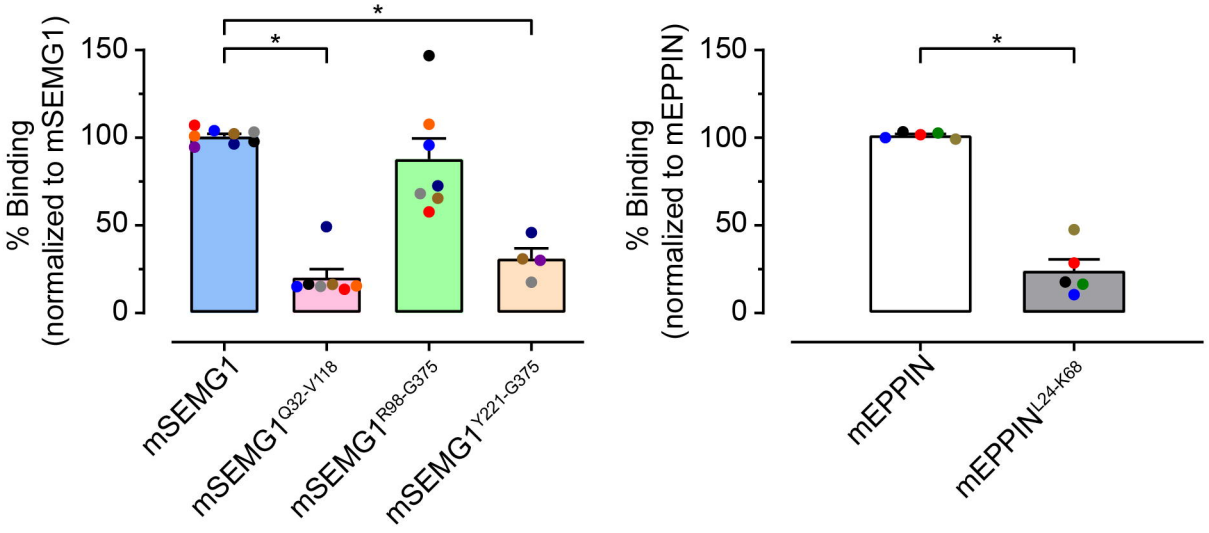
% Binding
(normalized to mSEMG1)
mSEMG1
mSEMG1 Q32-V118
mSEMG1 R98-G375
mSEMG1 Y221-G375
% Binding
(normalized to mEPPIN)
mEPPIN
mEPPIN L24-K68
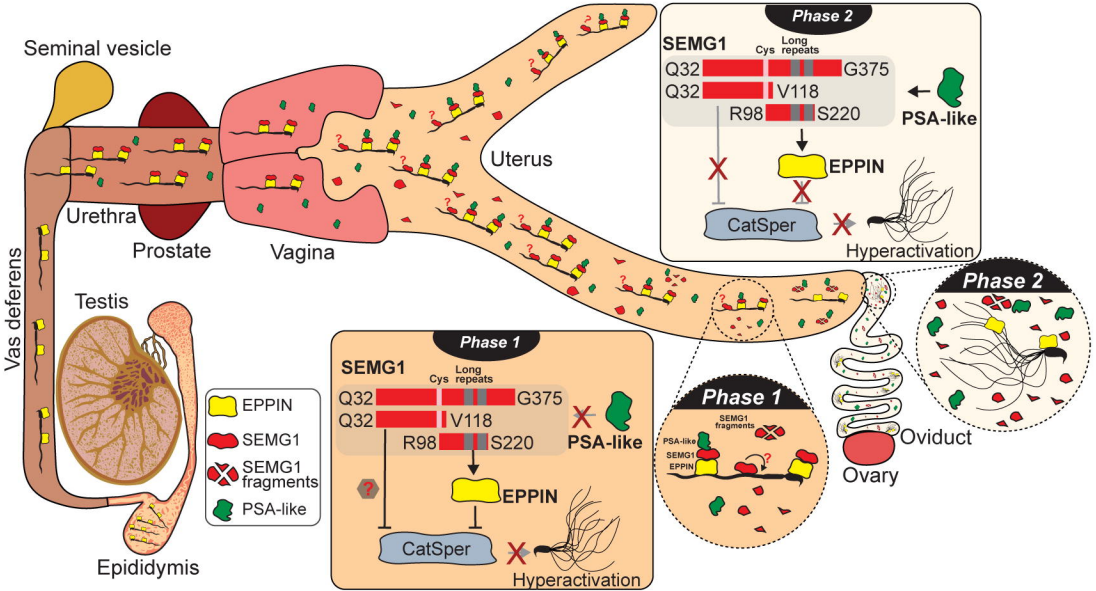
Mariani et al. Figure 7